AWARD NUMBER: W81XWH-19-1-0721

TITLE: Characterizing the Aggressiveness of Prostate Cancer with Multimodality Imaging

PRINCIPAL INVESTIGATOR: Prof. Timothy J. Scholl

CONTRACTING ORGANIZATION: University of Western Ontario, London, England

REPORT DATE: October 2021

TYPE OF REPORT: Annual

PREPARED FOR: U.S. Army Medical Research and Development Command
Fort Detrick, Maryland 21702-5012

REPORT DOCUMENTATION PAGE

Form Approved
OMB No. 0704-0188

1. REPORT DATE	2. REPORT TYPE	3. DATES COVERED
October 2021	Annual	01Sep2020-31Aug2021

4. TITLE AND SUBTITLE

Characterizing the Aggressiveness of Prostate Cancer with Multimodality Imaging

5a. CONTRACT NUMBER

5b. GRANT NUMBER
GRANT12713766

5c. PROGRAM ELEMENT NUMBER

6. AUTHOR(S)
Prof. Timothy J. Scholl, Ph.D.

E-Mail: scholl@uwo.ca

5d. PROJECT NUMBER

5e. TASK NUMBER

5f. WORK UNIT NUMBER

7. NAME AND ADDRESS OF CONTRACTOR
UNIVERSITY OF WESTERN ONTARIO, THE
WESTERN UNIVERSITY
1151 RICHMOND ST SUITE 2
LONDON N6A 5B8

8. PERFORMING ORGANIZATION REPORT NUMBER

9. SPONSORING / MONITORING AGENCY NAME(S) AND ADDRESS(ES)

U.S. Army Medical Research and Development Command
Fort Detrick, Maryland 21702-5012

10. SPONSOR/MONITOR'S ACRONYM(S)

11. SPONSOR/MONITOR'S REPORT NUMBER(S)

12. DISTRIBUTION / AVAILABILITY STATEMENT

Approved for Public Release; Distribution Unlimited

13. SUPPLEMENTARY NOTES

14. ABSTRACT

The goal of this research project is to demonstrate the ability of multimodality imaging to improve detection of prostate tumors and accurately determine their aggressiveness by comparing non-invasive molecular imaging to pathological examination. This project will study a total of 45 men with biopsy-proven prostate cancer. Prior to prostatectomy, they will undergo molecular imaging. After prostatectomy, sections of their prostates will be examined under a microscope by a pathologist for comparison with imaging data.

Year 1 Progress:

HREB paperwork completed; HRPO submission completed; Evaluation of sodium RF hardware and pulse sequence; Pathologist recruitment

Year 2 Progress:

Patient recruitment impacted by COVID-19 (1 study patient recruited to date); graduate student recruited; no-cost extension for third year has been filed with USAMRAA

15. SUBJECT TERMS
prostate cancer, multi-modality imaging, MRI, PET, tissue sodium concentration, prostate specific membrane antigen, prostatectomy biopsy, tumour aggressiveness, Gleason grade

16. SECURITY CLASSIFICATION OF:			17. LIMITATION OF ABSTRACT	18. NUMBER OF PAGES	19a. NAME OF RESPONSIBLE PERSON
a. REPORT	b. ABSTRACT	c. THIS PAGE			USAMRMC
Unclassified	Unclassified	Unclassified	Unclassified	33	19b. TELEPHONE NUMBER *(include area code)*

TABLE OF CONTENTS

1) INTRODUCTION

The title of this research project is “Characterizing the Aggressiveness of Prostate Cancer with Multi-Modality Imaging”. Its goal is to demonstrate the ability of multimodality imaging to improve detection of prostate tumors and accurately determine their aggressiveness by comparing non-invasive molecular imaging to pathological examination. This project will study a total of 45 men with biopsy-proven prostate cancer. Prior to prostatectomy, they will undergo molecular imaging. After surgery, sections of their prostates will be examined under a microscope by a pathologist. This examination is the gold-standard for characterizing tumors and will be used to establish how accurately the pre-surgical multimodality imaging assay was able to find tumors and predict their aggressiveness.

This research is being undertaken at the Robarts Research Institute at Western University and the Lawson Health Research Institute at St. Joseph’s Health Care, in London, Ontario, Canada. Our team is comprised of the following researchers:

Principal Investigators:

Timothy Scholl, PhD	Dept. of Medical Biophysics
Jonathan Thiessen, PhD	Dept. of Medical Biophysics
Glenn Bauman, MD	Dept. of Oncology
Aaron Ward, PhD	Dept. of Medical Biophysics

Co-Investigators:

Joseph Chin, MD	Dept. of Surgical Oncology
Stephen Pautler, MD	Dept. of Surgical Oncology
Nicholas Power, MD	Dept. of Surgical Oncology
Dr. Melissa Huynh	Dept. of Surgical Oncology (added 08/2021)
Zahra Kassam, MD	Dept. of Medical Imaging
William Pavlosky, MD	Dept. of Radiology and Nuclear Medicine
Madeleine Moussa, MD	Dept. of Pathology and Laboratory Medicine
Robert Bartha, PhD	Dept. of Medical Biophysics
Wenqing He, PhD	Dept. of Statistical and Actuarial Science

These investigators are employed at Western University and/or with the London Health Sciences Centre (London hospital network). They are not drawing any salary or remuneration from this project.

In addition, this project is supporting a full-time research pathologist, Dr. Mena Gaed, MD and a PhD student, Ms. Josephine Tan, MSc who is analyzing the imaging data.

Back to Table of Contents

2) KEYWORDS

prostate cancer
multi-modality imaging
magnetic resonance imaging
positron emission tomography
tissue sodium concentration
prostate specific membrane antigen
prostatectomy
biopsy
histopathology
tumour aggressiveness
Gleason grade

3) ACCOMPLISHMENTS

- **Major goals for Year 1**
  - Filing paperwork with Human Review Ethics Board.
  - Submission of HRPO documents.
  - Subtask 1: Evaluation of RF hardware.
    Evaluation of Sodium MRI pulse sequences.
    Manuscript preparation.
  - Graduate student recruitment.
  - Pathology Assistant recruitment.
  - Subtask 2: Recruitment of first study patients.
    Human imaging acquisition
- **What was accomplished under these goals?**
  - HREB paperwork submitted and approval received.
  - HRPO completed for submission October 2020.
  - Subtask 1: Evaluation of sodium RF hardware

    Experiments to assess imaging performance were undertaken by comparing sodium signal acquired at St. Joseph's hybrid PET/MRI (Biograph mMR, Siemens) to Robarts 3T MRI (Discovery MR750 3T, GE Healthcare). Free-induction decay measurements were acquired using a phantom containing 100 mM sodium and identical RF coils at both sites. Signal-to-noise ratios (SNR) were identical across sites for the same acquisition parameters. This validates that the sodium MR imaging performance demonstrated in our preliminary study† at the Robarts Research Institute has been achieved for the first time at the combined PET/MRI hybrid system. (†Broeke NC, *et al*., *Characterization of clinical human prostate cancer lesions using 3.0-T sodium MRI registered to Gleason-graded whole-mount histopathology.* Journal of Magnetic Resonance Imaging, 2019. **49**(5): p. 1409-1419. Manuscript has been appended to report)
  - Subtask 1: Pulse sequence development

    A pulse sequence known as "density-adapted 3D projection reconstruction" was acquired via site-to-site transfer from our collaborator, Armin Nagel (MRI Physics Group University Hospital, Erlangen, Germany). Professor Nagel is an expert in sodium MRI and has developed this pulse sequence for efficient *in vivo* 3D sodium imaging (Nagel AM, *et al*., *Sodium MRI using a density-adapted 3D radial acquisition technique*. Magnetic Resonance in Medicine, 2009. **62**(6): p. 1565-1573). This pulse sequence is a series of instructions for the MRI to collect an image. They were compiled for the Biograph mMR hybrid PET/MRI scanner. Imaging SNR was compared with a similar radial sequence separately developed by Alireza Akbari for the GE Discovery MR750 3T using a phantom and identical acquisition parameters. This validates the pulse sequence implementation.

- Subtask 1: Manuscript preparation.

  The RF hardware, which was developed for this project is being described in a manuscript for submission in NMR in Biomedicine. This manuscript is being written by Mr. Adam Farag, the PhD student working on this project as part of his thesis. This manuscript will include exemplary PET and MRI (proton and sodium) images. This will be acquired with the first human volunteer later this fall.
- PhD student (Josephine Tam) was recruited but could not join project in Year 1 due to COVID-19 pandemic. This graduate student will join project in 2021. A second PhD student (Adam Farag) is currently training in this project.
- Dr. Mena Gaed is a pathologist with significant experience in preparation of whole-mount prostate sections and prostate lesion grading. He has been salaried for the duration of this project and will process tissue specimens, grade lesions and co-register *in vivo*/*ex vivo* imaging data.
- Subtask 2: Recruitment of first study patients.

  Patient recruitment for this study was not possible due to suspension of all medical research at Ontario hospitals due to Provincial guidelines. Recruitment will begin Fall 2020.
- Subtask 2: Human imaging acquisition.

  Unanticipated delays have been encountered which have prevented us from acquiring human imaging data. These include a change of radio-labeled PET tracer, which required a new application to Heath Canada; moratorium on hospital and university research by the Province of Ontario; final submission of the HRPO documentation. *The moratorium on research and delays in submission of the HRPO documentation were related to the COVID-19 pandemic, which prevented us from recruiting patients and completion of our paperwork.*

- **Opportunities for training and professional development.**
  - Mr. Adam Farag is currently working on this research project as part of his PhD thesis in Medical Biophysics at Western University.
- **How were the results disseminated to communities of interest?**
  - No human imaging has been undertaken due to COVID-19 delays. A manuscript describing the novel RF hardware is being written and will be submitted to a journal for publication after peer review.
- **What do you plan to do during the next reporting period to accomplish the goals?**
  - We expect that the first human subjects will be recruited for imaging experiments in the Fall of 2020.

- **Major goals for Year 2**
  - Molecular imaging of human prostate cancer
  - Subtask 1: Recruitment and imaging of 16 patients to research study.

Human imaging acquisition with multiparametric MRI, sodium MRI and PSMA PET

- **What was accomplished under these goals?**
  - Subtask 1: Patient recruitment and imaging

    Patient recruitment into this study has been significantly hampered by provincial health restrictions. After provincial restrictions lasting from 12/26/2020 to 02/16/2021 were lifted, the first study patient was recruited and imaged on 02/23/21 (See Figure 2). The Province of Ontario soon entered another lockdown on 03/04/2021 and the resulting research moratorium prevented us from recruiting any further patients. (See CHANGES/PROBLEMS regarding the unforeseen impediments to patient recruitment.)
  - PhD student (Josephine Tam) was recruited to this research project and began her graduate training on 01/01/2021. PhD student, Adam Farag completed his PhD and has graduate. He is no longer involved with this project.
  - Mrs. Stephanie Horst has left her position as clinical coordinator and patient recruiter for the urological surgeons, Drs. Chin, Pautler and Power. Our research pathologist, Dr. Mena Gaed has taken on the responsibility of patient recruitment for this study and is actively seeking consent from patients under the clinical care of our surgeons.
- **Opportunities for training and professional development.**
  - Mr. Adam Farag, a PhD trainee, helped to evaluate the RF hardware and has now graduated. He is currently working for Siemens Canada at the hybrid PET/MRI facility at University Health Network in Toronto.
  - Ms. Josephine Tan, a new PhD trainee has joined this research project on 01/01/2021. She has a MSc from the University of Toronto in Medical Biophysics and will be analyzing the imaging data from this study as part of her PhD training.
- **How were the results disseminated to communities of interest?**
  - At this juncture only one patient in this study has been recruited and imaged due to COVID-19 delays that have impacted recruitment. These delays are beyond our ability to control. We are waiting to complete at least two more imaging subjects prior to publishing our initial results.
  - Preliminary results from our first human subject will be presented by PhD trainee, Josephine Tan at the World Molecular Imaging Congress (October 5-8, 2021) as a poster. This scientific meeting is being held virtually this year due to COVID-19.
- **What do you plan to do during the next reporting period to accomplish the goals?**
  - At present, the fourth wave of COVID-19, which is being driven by the Delta Variant in under-vaccinated persons is under relative control in Ontario. The province has mandated proof of vaccination for access to non-essential services beginning 09/22/2021 and as of 10/22/21, vaccine passports will be implemented province wide. We hope that this will prevent another full lock down, which would halt our research yet again.

- The urological surgeons have been queried to verify that they have regained access to surgical dates for prostatectomy. They have indicated that, on average, as a group they will be performing ~15 prostatectomies per month, and we should expect to be able to recruit 2 to 3 patients per month moving forward.
- To improve our uptake of consenting patients, we have expanded our list of recruiting surgeons to include Dr. Melissa Huynh.
- Our research pathologist, Dr. Mena Gaed has taken on the responsibility of patient recruitment for this study and is actively seeking consent from patients under the clinical care of our surgeons. As this is written, he has identified two patients meeting criteria for our study and awaiting surgical dates.
- To improve the uptake of our imaging among potential patients, we have been working on second-generation RF technology to replace the sodium/proton endorectal RF coil. This RF coil is currently placed in the rectum and has been off-putting for some patients. The new RF coil will be a larger external surface coil obviating the need for insertion and increasing patient comfort for the hour-long imaging session. Early sodium results from an external RF coil are shown in Figure 3. The new RF setup is producing more uniform coverage of the prostate for sodium MRI, and we are improving the available SNR by increasing the number and geometry of the surface coil windings. This development is outside the initial SOW; however, our team has felt that during our hiatus from human research as a result of COVID-19, we should redirect our research focus to improving our imaging technology so that the resulting imaging data would be of higher quality.
- In addition, we have worked to further refine the DA3DPR imaging sequence for sodium MRI. This work is being undertaken at the Robarts Research Institute MRI. Improvements to the sequence have been evaluated in tissue-mimicking phantoms and in rodents using an animal protocol held by Scholl. This work is also outside the scope of the SOW for Year 2 but again, this progress will ultimately benefit our imaging study and development of software and hardware has not been as affected by the pandemic since it has not involved human subjects to date.

4) IMPACT

- **What was the impact on the development of the principal discipline(s) of the project?**
  Nothing significant to report at this juncture.
- **What was the impact on other disciplines?**
  Nothing significant to report at this juncture.
- **What was the impact on technology transfer?**
  Nothing significant to report at this juncture.
- **What was the impact on society beyond science and technology?**
  Nothing significant to report at this juncture.

5) CHANGES/PROBLEMS

- **Changes in approach and reasons for change (Year 1)**
  - We have changed the original radio-labeled PET tracer from [^{18}F]DCFPyL to PSMA-1007. Licencing for production of [^{18}F]DCFPyL from the Centre for Probe Development and Commercialization (CPDC) in Hamilton, ON will cease in 2021 and we determined that it was preferable to complete the entire study using the newer PET tracer, PSMA-1007, which is reported to have more specificity than ^{18}F]DCFPyL. This PET tracer will ultimately be produced at the St. Joseph's cyclotron in London under licence from the CPDC. This technical change to our study has already been submitted to Health Canada and approval has been received to use PSMA-1007. This has caused a short delay in our research timeline. Cost and availability for the new tracer remain unchanged.

- **Actual or anticipated problems or delays and actions or plans to resolve them**

  COVID-19 Impact on Research Project (Years 1 & 2)

  It is important to note that the impact of COVID-19 on society and the response to this pandemic is significantly different in Canada compared with what has been apparent on the American news. Compared with the experience in the US, it is possible that the impact on our socialized health care system has been more significant. It has been estimated by the Ontario Medical Association that the COVID-19 pandemic has left a backlog of 15.9 million surgeries, diagnostic exams, screenings and other medical procedures that should otherwise have been performed in Ontario (CBC News Article 06/09/2021). Conservative estimates of the number of cancelled surgeries in Canada by spring 2021 have topped 350,000 to free up critical care beds for COVID patients. Exact numbers are uncertain, but these cancellations include prostatectomies, and as a result, many men have been placed on hormone therapy in lieu of immediate treatment. These men are not candidates for this imaging study (see below). While this health care situation does sound bleak, the Province of Ontario has announced that they will increase direct funding to hospitals by an amount of $324 million to increase capacities at hospitals to 115% to clear surgical backlogs resulting from COVID (CBC News Article 07/28/2021).

  Decisions by our health authorities and politicians have prompted extended stay-at-home orders for Ontario during the first three waves of the pandemic. During these shutdowns, our ability to conduct human research has been hindered and only recently have we been able to gain research access for our study. This situation has beyond the control of the researchers who have committed their time and effort to this project; however, we remain committed to recruiting as many patients as possible to this study and confident that by

the end of this project we will be able to demonstrate that this technology has clinical utility.

- *COVID-19 has seriously impacted our progress with this project over the last 18 months.* See Figure 1 of the Appendices for historical data on COVID-19 cases reported in the Province of Ontario since the onset of the pandemic. Details regarding public health measures and lockdowns during the pandemic have been provided below.

  First COVID-19 Wave
  - In its first response to the first wave of the COVID-19 pandemic, the Province of Ontario imposed health measures lasting from 03/2020 to 09/2020, which barred our access to the hospital and our imaging infrastructure. This obviously prevented us from recruiting patients to our research study. In September 2020, biomedical research in university laboratories was able to resume with reduced occupancy limits (first 20%, then 30 % and finally 60% of normal) but research access to PET/MRI at the hospital was still restricted. Further impacting our study, Ontario hospital resources were overwhelmed with COVID-19 patients and non-emergent surgeries (*including prostatectomies*) and other procedures were placed on hold to free-up much-needed hospital beds to care for COVID-19 patients. As a result, prostatectomies were cancelled through much of 2020/21, and these patients were placed on hormone therapy to await possible further treatment after the pandemic passed.

  Second COVID-19 Wave
  - Ontario was placed in a second lock-down from 12/26/2020 to 02/16/2021. Again, access to research infrastructure was not possible. Finally, in the valley between the second and third waves of COVID, we were able to recruit the first patient to our study who received imaging on 02/23/21. These results are presented in Figure 2.

  Third COVID-19 Wave
  - Ontario entered a third lockdown on 03/04/21 in response to rapidly rising rates of new infections. This was largely due to the slow arrival of vaccines in Canada in early 2021 compared with the rollout in the United States and the increasing prevalence of the highly infectious Delta Variant. Again, our human imaging research was idled. Ontario began lifting restrictions on 06/02/21 in *three* steps (https://www.ontario.ca/page/reopening-ontario). The province has determined that the current third step, which began 07/16/21, will continue indefinitely.

  - While the current health measures of the third stage have allowed us to return to our clinical research, there are still significant hurdles facing our research project regarding patient recruitment. At this juncture, our urological surgeons are just now resuming some regular scheduling of

prostatectomies as surgical times become available on a limited basis at area hospitals. Compared with pre-COVID surgical numbers, the current schedule is still limiting, and surgical dates can only be confirmed less than one week out. This is problematic for our project where we image these men prior to prostatectomy. At present, the radioactive PET tracer for our imaging is being produced at a cyclotron in Toronto (2 hours away) once a week (on Tuesdays) for the entire province and is delivered that morning to our hospital in London. Note that they require one week's notice for this service, which normally isn't a problem if we can reliably schedule our imaging studies at least a couple of weeks in advance.

- It has also been difficult to recruit patients into our study. This is a result of three factors, limited surgical availability as described above, patient hesitancy to participate in this study during COVID and the backlog of patients who were placed on hormone therapy, now being triaged for surgical intervention. While hormone therapy is obviously helpful for the patient, it makes accurate Gleason grading of the disease during pathology impossible. As a result, these men are not eligible for our study as we require whole-mount histopathology as our gold-standard for comparison with MRI and PET imaging data. Thus, the pool of patients available for our study is currently limited but our surgical collaborators estimate that we should be able to recruit 2 to 3 subjects per month as these problems resolve during the 4th quarter of 2021.

<u>Fourth COVID-19 Wave</u>

- At present, Ontario (and most of Canada) is in the midst of a fourth wave of the COVID-19 pandemic. This resurgence has been driven primarily by infection with the more transmissible Delta Variant among the portion of the population that is either unvaccinated and those who have only received one vaccine dose. Currently, 75% of eligible Ontarians have received one vaccine dose and 70% have receive two doses. The Province of Ontario has recently mandated a vaccination passport to help curb the transmission of the Delta Variant of COVID, mostly by the unvaccinated. We are hoping that this passport will further incentivize vaccine-hesitant individuals to become vaccinated and this will help control the fourth wave of the pandemic in our province. If this plays out, we will be able to salvage this research project.

- **Changes that had a significant impact on expenditures**
  - None.
- **Significant changes in use or care of human subjects, vertebrate animals, biohazards, and/or select agents**
  - None.
- **Significant changes in use or care of human subjects**
  - None.

- **Significant changes in use or care of vertebrate animals**
  - None.
- **Significant changes in use of biohazards and/or select agents**
  - See earlier discussion of use of a new PET tracer, PSMA-1007 to replace [^{18}F]DCFPyL.

6. PRODUCTS

- Publications, conference papers, and presentations
    - Preliminary results from our first human subject will be presented by PhD trainee, Josephine Tan at the World Molecular Imaging Congress (October 5-8, 2021) as a poster. This scientific meeting is being held virtually this year due to COVID-19.
- Website(s) or other Internet site(s)
    - Nothing to report.
- Technologies or techniques
    - Nothing to report.
- Inventions, patent applications, and/or licences
    - Nothing to report.
- Other Products
    - Nothing to report.

7. PARTICIPANTS & OTHER COLLABORATING ORGANIZATIONS

- **What individuals have worked on the project?**

The following individuals have worked on this project in Years 1 and 2. (This list will expand to include other individuals named in the project who have yet to participate until patients are recruited.)

Name:	Timothy Scholl, PhD
Project Role:	Nominated Principal Investigator
Researcher Identifier:	I-6178-2012 (Publons)
Nearest person month worked:	6 months (continuing)
Contribution to Project:	Project oversight and administration
Funding Support:	University faculty
Name:	Jonathan Thiessen, PhD
Project Role:	Principal Investigator
Researcher Identifier:	B-3514-2015 (Publons)
Nearest person month worked:	6 months (continuing)
Contribution to Project:	Hybrid PET/MRI
Funding Support:	Hospital scientist and university faculty
Name:	Glenn Bauman, MD
Project Role:	Principal Investigator
Researcher Identifier:	D-5986-2011 (Publons)
Nearest person month worked:	1 month (continuing)
Contribution to Project:	Clinical oversight of study
Funding Support:	Hospital physician and university faculty
Name:	Aaron Ward, PhD
Project Role:	Principal Investigator
Researcher Identifier:	B-4950-2015 (Publons)
Nearest person month worked:	1 month (continuing)
Contribution to Project:	Co-registration of imaging data
Funding Support:	University faculty
Name:	Joseph Chin, MD
Project Role:	Co-Investigator
Researcher Identifier:	
Nearest person month worked:	1 month (continuing)
Contribution to Project:	Recruitment of patient and surgery
Funding Support:	Hospital physician and university faculty
Name:	Matthew Fox, PhD
Project Role:	Research Assistant

Researcher Identifier:	
Nearest person month worked:	6 months (continuing)
Contribution to Project:	Evaluation of PET/MRI imaging hardware
Funding Support:	Other, outside this project
Name:	Alireza Akbari, PhD
Project Role:	Research Assistant
Researcher Identifier:	
Nearest person month worked:	6 months (continuing)
Contribution to Project:	Sodium MRI pulse sequence and hardware
Funding Support:	Other, outside this project
Name:	Josephine Tan, MSc
Project Role:	PhD student
Researcher Identifier:	
Nearest person month worked:	9 months (continuing)
Contribution to Project:	Thesis project, analysis of imaging data
Funding Support:	This project (100%)
Name:	Adam Farag, MSc
Project Role:	PhD student
Researcher Identifier:	
Nearest person month worked:	2 months (completed)
Contribution to Project:	RF hardware integration
Funding Support:	This project (25%)
Name:	Mena Gaed
Project Role:	Pathologist
Researcher Identifier:	
Nearest person month worked:	6 months (continuing)
Contribution to Project:	Recruitment, pathology, and lesion grading
Funding Support:	This project (100%)
Name:	Stephanie Horst
Project Role:	Research Coordinator
Researcher Identifier:	
Nearest person month worked:	6 months (continuing)
Contribution to Project:	Patient recruitment
Funding Support:	This project (10%)
Name:	Catherine Hildebrand
Project Role:	Research Coordinator
Researcher Identifier:	
Nearest person month worked:	6 months (continuing)
Contribution to Project:	Ethics paperwork etc.

Funding Support:	This project (5%)

- **Has there been a change in the active other support of the PD/PIs or senior/ley personnel since the last reporting period?**
  - No.
- **What other organizations were involved as partners?**
  - None.
- **Locations of organization**
  - Not applicable.
- **Partners contribution to the project**
  - Not applicable.

8. SPECIAL REPORTING REQUIREMENTS

- Collaborative Awards
  - None.
- Quad Charts
  - None.

9) APPENDICES

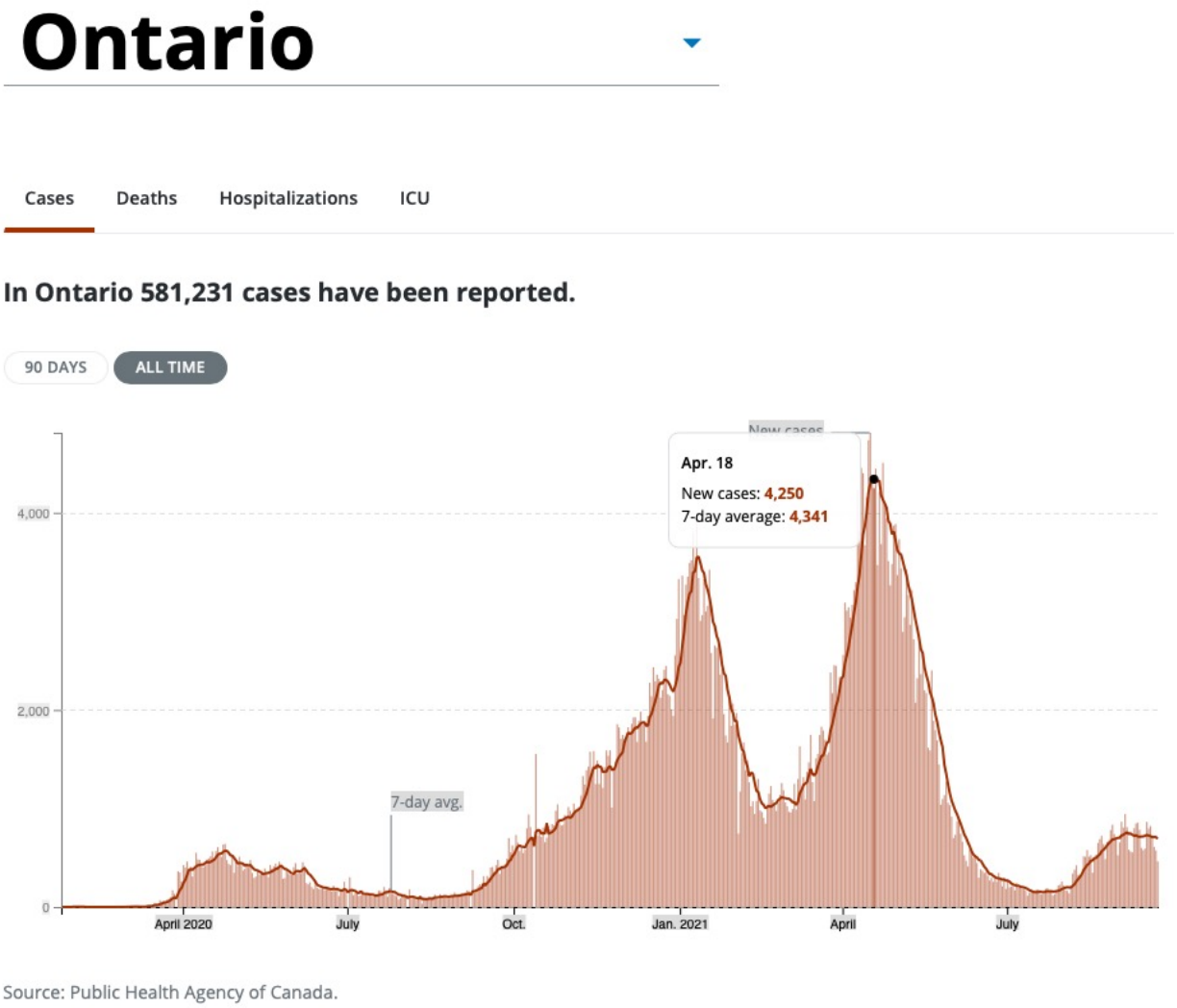

Figure 1: *Daily new COVID-19 cases reported in the Province of Ontario (2020-present)*. Since 02/2020, there have been four waves of COVID-related cases in this province including the current resurgence. For a complete description of the impact of COVID-19 on this research study see Section 5. CHALLENGES/PROBLEMS. (Note: the amplitude of the first wave has likely been underestimated due to limited testing available in Ontario at the onset of the pandemic.)

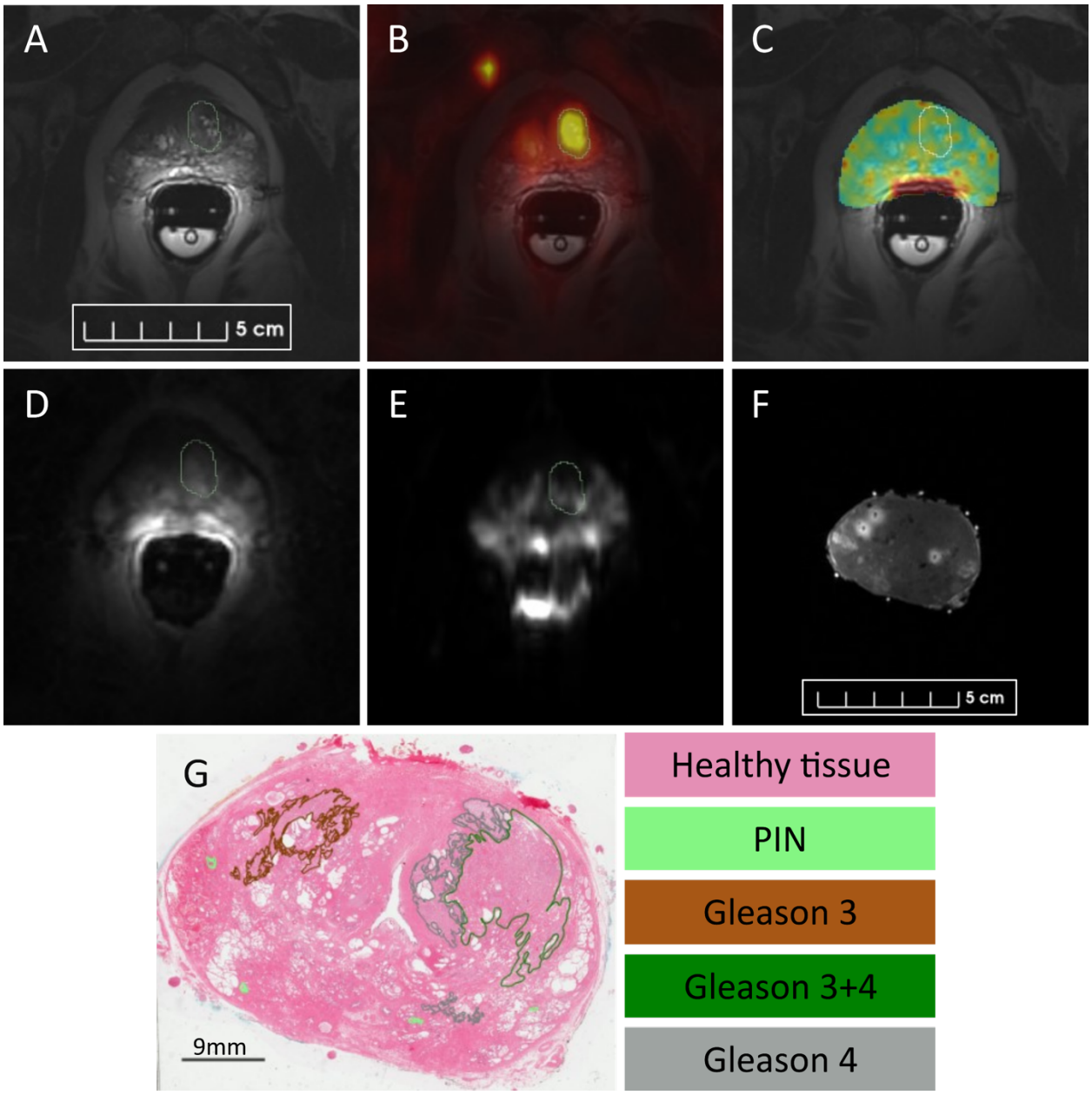

Figure 2: *Representative images from the first patient* (62 years old, 95.2 kg, Gleason score=7): (A) T_2-weighted MRI, (B) co-registered [^{18}F]PSMA-1007 PET, (C) ^{23}Na MRI (the raw sodium signal is averaged from 5 acquisitions and has been segmented to the prostate), (D) dynamic contrast-enhanced MRI, (E) and the apparent diffusion coefficient map. The green outline represents the primary lesion segmentation defined by 40% SUV_{max}. (F) Ex vivo T_1-weighted MRI shows the 3 internal and 7 external fiducials on the prostate specimen. (G) Digitized whole-mount histopathology shows the Gleason contours (green: Gleason grade 3, gray: Gleason grade 4, green: Gleason grade 3+4, light green: prostatic intraepithelial neoplasia [PIN]).

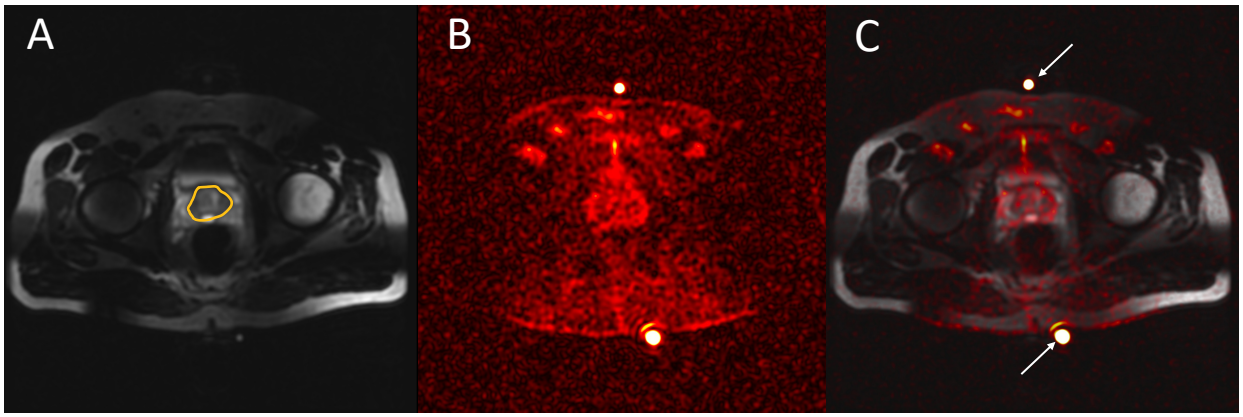

Figure 3: *Development of external RF surface coils for sodium imaging of the prostate.*

(A) The prostate has been outlined in yellow on the T_2-weighted proton image.

(B) Sodium signal from external RF surface coils. Nominal voxel size is 3 mm by 3 mm in plane by 8 mm out of plane. Acquisition time: 30 minutes. Measured SNR is ~8.

(C) Overlay of the sodium signal on axial T_2-weighted proton image through the prostate. The proton image was acquired using the proton body coil at 3T.

A novel butterfly RF coil was built and tested for sodium MRI. This coil consisted of two 18-cm diameter RF loops arranged as a figure eight with one lobe placed under the patient and the other above the prostate over the abdomen. Compared with the existing endorectal (ER) surface RF coil, the butterfly coil has the advantage of being non-invasive and provides more uniform imaging sensitivity for entire prostate. However, this comes at the expense of reduced signal-to-noise ratio. Further effort is underway to improve the sensitivity of a non-invasive external surface coil but at present, the existing dual-frequency ER RF coil is being used for clinical imaging. (Note: the circular objects identified by arrows in panel (C) are external calibration vials.)

ORIGINAL RESEARCH

Characterization of Clinical Human Prostate Cancer Lesions Using 3.0-T Sodium MRI Registered to Gleason-Graded Whole-Mount Histopathology

Nolan C. Broeke, MSc,[1] Justin Peterson, MSc,[1] Joseph Lee, BSc,[1] Peter R. Martin, PhD,[1] Adam Farag, MSc,[2] Jose A. Gomez, MD,[3] Madeleine Moussa, MD,[3] Mena Gaed, MD,[3] Joseph Chin, MD,[4,5] Stephen E. Pautler, MD,[4,5] Aaron Ward, PhD,[1,5] Glenn Bauman, MD,[1,5] Robert Bartha, PhD,[1,2,6] and Timothy J. Scholl, PhD[1,2,7]*

Background: Overtreatment of prostate cancer (PCa) is a healthcare issue. Development of noninvasive imaging tools for improved characterization of prostate lesions might reduce overtreatment.
Purpose: To measure the distribution of tissue sodium concentration (TSC), proton T_2-weighted signal, and apparent diffusion coefficient (ADC) values in human PCa and to test the presence of a correlation between regional differences in imaging metrics and the Gleason grade of lesions determined from histopathology.
Study Type: Cross-sectional.
Subjects: Ten men with biopsy-proven PCa.
Sequences/Field Strength: Sodium, proton T_2-weighted, and diffusion-weighted MRI data were acquired using Broad-Band 3D-Fast-Gradient-Recalled, 3D Cube (Isotropic 3D-Fast-Turbo-Spin-Echo acquisition) and 2D Spin-Echo sequences, respectively, with a 3.0T MR scanner.
Assessment: All imaging data were coregistered to Gleason-graded postprostatectomy histology, as the standard for prostate cancer lesion characterization. Regional TSC and T_2 data were assessed using percent changes from healthy tissue of the same patient (denoted ΔTSC, ΔT_2).
Statistics: Differences in ΔTSC, ADC, and ΔT_2 as a function of Gleason score were analyzed for each imaging contrast using a one-way analysis of variance or a nonparametric *t*-test. Correlations between imaging data measures and Gleason score were assessed using a Spearman's ranked correlation.
Results: Evaluation of the correlation of ΔTSC, ADC, and ΔT_2 datasets with Gleason scoring revealed that only the correlation between ΔTSC and Gleason score was statistically significant ($r_s = 0.791$, $p < 0.01$), whereas the correlations of ADC and ΔT_2 with Gleason score were not ($r_s = -0.306$, $p = 0.079$ and $r_s = -0.069$, $p = 0.699$, respectively). In addition, all individual patients showed monotonically increasing ΔTSC with Gleason score.
Data Conclusion: The results of this preliminary study suggest that changes in TSC, assessed by sodium MRI, has utility as a noninvasive imaging assay to accurately characterize PCa lesions. Sodium MRI may provide useful complementary information on mpMRI, which may assist the decision-making of men choosing either active surveillance or treatment.
Level of Evidence: 1
Technical Efficacy: Stage 2

J. MAGN. RESON. IMAGING 2019;49:1409–1419.

View this article online at wileyonlinelibrary.com. DOI: 10.1002/jmri.26336

Received Jun 11, 2018, Accepted for publication Aug 24, 2018.

*Address reprint requests to: T.J.S., 1151 Richmond Street North, London, ON, Canada, N6A 5B7. E-mail: scholl@uwo.ca

[Correction added on December 28, 2018, after first online publication: Adam Farag's degree was updated. [Correction added on January 11, 2019, after first online publication: The middle initial of author Peter Martin was corrected from "A." to "R."]]

From the [1]Department of Medical Biophysics, Western University, London, ON, Canada; [2]Robarts Research Institute, Western University, London, ON, Canada; [3]Department of Pathology and Laboratory Medicine, Western University, London, ON, Canada; [4]Department of Surgery, Western University, London, ON, Canada; [5]Department of Oncology, Western University, London, ON, Canada; [6]Departments of Medical Imaging and Psychiatry, Western University, London, ON, Canada; and [7]Ontario Institute for Cancer Research, Toronto, ON, Canada

Additional supporting information may be found in the online version of this article.

One in seven men will develop prostate cancer (PCa) in their lifetime, making it the most common noncutaneous malignancy in males.[1] However, not all disease progresses and therefore diagnosis of clinically insignificant disease has been a concern since the introduction of the prostate-specific antigen (PSA) screening test.[2,3] Overdiagnosis has been shown to negatively affect patient quality of life and increase the societal healthcare costs.[4] For men with suspected PCa, a standard approach involves a transrectal ultrasound (TRUS)-guided biopsy to extract 12 cores[5] for histological Gleason scoring. The current system for grading PCa is Grade Grouping based on Gleason scores.[6] A Gleason score displays the primary and secondary cancer grades present in a patient, and is inherently related to tumor aggression; making the Gleason score the strongest prognostic and predictive factor for the disease.[7] However, the biopsy samples ~0.2% of the prostate, which carries a 30–40% risk of undersampling clinically significant lesions.[8–10] Therefore, the use of nonsurgical imaging-based methods to accurately discriminate between low- and high-grade lesions would be useful to reduce repeated negative biopsies, to place patients in the proper treatment streams, and to assist in active surveillance of low-risk cancer. This, in turn, will optimize patient outcomes and the use of healthcare resources. Currently, multiparametric magnetic resonance imaging (mpMRI) contrasts such as T_2-weighted, diffusion-weighted magnetic resonance imaging (DWI-MRI), and dynamic contrast-enhanced MRI (DCE-MRI) aid physicians in PCa lesion detection.[11–13] DWI signal intensity is based on measurement of the Brownian motion of water molecules in a voxel.[14] Inverse correlations between apparent diffusion coefficient (ADC) signal intensity and cell count in tumors were shown by Surov et al.[15] The strength of these correlations was seen to be dependent on the location of the cancer tissue, with only moderate inverse correlations recorded in prostatic cancer.[15] T_2-weighted prostate MRI produces anatomical images with high spatial resolution and it allows for precise differentiation of the different zones of this gland. On T_2-weighted images of the prostate, lesions in the peripheral zone typically show a hypointense signal compared to healthy tissue.[12] The degree of these differences can vary with Gleason score. However, regions of lower signal do not necessarily represent malignancies. Prostate lesions arising from scars, atrophy, hyperplasia, chronic prostatitis, and postbiopsy hemorrhage have been shown to also exhibit low signal intensity on T_2-weighted images.[16]

T_2-weighted imaging and ADC values provide high spatial resolution but their specificity is often insufficient to localize malignant lesions and confidently assign tumor grades to these foci. Thus, there is a need for additional imaging biomarkers to provide complementary information about the location and grade of intraprostatic cancer. Tissue sodium concentration (TSC) has been shown to be a sensitive indicator of cell integrity and energy metabolism.[17,18] The link between increased activity of a sodium-proton (Na^+/H^+) antiport[19,20] and sodium-potassium (Na^+/K^+) ATPase[17,21] and tumor malignancy has been well studied. TSC measured by sodium (Na) MRI can provide regional information about intracellular and extracellular changes within tissue. TSC has previously been seen to be significantly elevated in brain and breast cancer.[18,22,23] However, the relationship between TSC and tumor grade in human PCa has not yet been analyzed. Our lab has previously developed sodium ion (^{23}Na) imaging hardware comprised of a transmit-only asymmetrical birdcage coil and a receive-only endorectal coil, providing sufficient sensitivity to image endogenous sodium in the prostate.[24]

Materials and Methods

Patients

Ten male patients (aged 63 ± 5 years) with biopsy-proven PCa, originally recruited for a larger study involving multimodality image-guided PCa therapy, volunteered for this additional imaging study prior to prostatectomy. All research was approved by the Institutional Review Board (the Health Sciences Research Ethics Board), and written informed consent was obtained from all patients.

Inclusion criteria for the original imaging study were intentionally chosen to target a patient population including low- to intermediate-risk groups, where additional characterization of tumor aggression would be particularly useful for risk stratification decisions and where mpMRI provides less reliable guidance. In addition to standard exclusion criteria for MR studies (implanted devices, etc.), men were excluded from this study if they had prior therapy for PCa, use of 5-alpha reductase inhibitors within 6 months of the start of the study, a prostate volume greater than 68 cc, allergies to contrast agents and other administered agents, insufficient renal function, and a residual bladder volume greater than 150 mL. Patients were instructed to drink 30 mL of milk of magnesia the night before the MR exam and to fast 12 hours prior to the exam to facilitate a clear colon. Sodium MRI was performed in combination with mpMRI, including the following contrasts: diffusion-weighted, T_2-weighted, and post-gadolinium T_1-weighted imaging; however, DCE was not included in the data analysis. Ex vivo imaging of the prostatectomy specimens included T_1- and T_2-weighted imaging.

In Vivo mpMRI

All MRI data for this study were acquired at a field strength of 3.0T (General Electric Healthcare Discovery MR750 3.0T, Milwaukee, WI). High-resolution T_2-weighted images (echo time [TE]: 162 msec, repetition time [TR]: 2000 msec, field of view (FOV): 140 × 140 mm, voxel size: 0.44 × 0.73 × 1.4 mm, flip angle: 90°) were acquired using a 3D Cube sequence, and the standard inflatable ^1H endorectal (ER) coil. This image set was used for registration of sodium images to histopathology. ADC maps were obtained using a 2D spin-echo sequence, the inflatable ^1H ER coil, and the following parameters: TE: 68.1 msec, TR: 5600 msec, FOV: 140 × 140 mm, voxel size: 1.1 × 0.55 × 3.6 mm, flip angle 90°, and *b*-values of 100 and 800 mm^2/s.

Sodium Imaging

Sodium imaging was preformed using a bespoke ER receive-only radiofrequency (RF) coil and an asymmetric transmit-only birdcage RF coil.[24] A topical anesthetic, Xylocaine (2%), was applied to the patient prior to insertion of the ER coil. Following insertion of the ^{23}Na ER coil a set of ^{1}H, axial T_2-weighted images were initially acquired using a 2D fast spin-echo sequence (TE: 139.2 msec, TR: 5300 msec, FOV: 140 × 140 mm, voxel size: 1.09 × 1.09 × 3 mm, and flip angle 90°) were acquired with the body ^{1}H RF coil to provide morphological context for the sodium images. This enabled accurate registration of the sodium images to the high-resolution T_2-weighted image set. ^{1}H imaging with the ^{23}Na hardware was possible because of the unshielded design of the transmit-only RF coil, along with proper detuning of the receive-only ER coil. Sodium images were then acquired using a broad-banded 3D fast gradient-recalled-echo sequence with the following parameters: TE: 1.5 msec, TR: 80 msec, FOV: 140 × 140 mm, voxel size: 4.4 × 4.4 × 6 mm, and flip angle: 85°, NEX: 10, NA: 5, scan time: ∼37 minutes. Three calibration vials containing 30, 90, and 150 mmol/L of sodium chloride solutions were incorporated into the rigid ^{23}Na ER coil. These solutions were used to obtain absolute in vivo sodium concentration by scaling the sodium signal from the prostate to known sodium concentrations in the ER coil. Sodium images were normalized to the sensitivity profile of the ^{23}Na ER surface coil, acquired in a separate measurement in a procedure described by Axel et al.[25] Using the method described by Farag et al,[24] regional maps of absolute TSC [mmol/L] were computed throughout the prostate from the normalized sodium images using the observed image intensity from the reference vials, which were incorporated into the ER coil.

Ex Vivo Imaging

Ex-vivo prostate MR images were acquired to facilitate accurate registration of in vivo prostate image data to histology. Following radical prostatectomy, prostate specimens were encased in a syringe of Christo-Lube MCG 1046 (Lubrication Technology, Franklin Furnace, OH), an MR-invisible fluorinated lubricant, to minimize magnetic susceptibility artifacts at the tissue–prostate boundary. The specimens were then imaged on the same 3T scanner used for in vivo imaging. Both T_1-weighted (TE: 2.34 msec, TR: 6.41, FOV: 140 × 140 mm, voxel size: 0.73 × 0.55 × 0.6 mm, flip angle: 15°) and T_2-weighted (TE: 114 msec, TR: 2000 msec, FOV: 140 × 140 mm, voxel size: 0.73 × 0.44 × 0.6 mm, and flip angle: 90°) images were obtained using a 3D spoiled gradient-recalled-echo and a 3D Cube sequence, respectively.

Whole-Mount Pathology

A detailed description of the preparation of the ex vivo prostates for histopathology can be found in Ref. 26. Dyed cotton threads, treated with a paramagnetic contrast agent, were used as MRI-visible fiducial prostate markers, which are also visible under microscopic examination. Excised prostate specimens were pierced with three cotton threads through the prostate and seven threads on the surface as fiducial markers. The prostate midglands were then sliced into ∼4-mm transverse sections before paraffin embedding, leaving enough of the apex and base to be sagittally sliced for routine pathology analysis. Using a microtome, a 4-μm slice was obtained from each section and stained with hematoxylin and eosin (H&E). The slides were then scanned at high resolution (0.5-μm isotropic resolution, 24-bit color) using a brightfield slide scanner (ScanScope GL; Aperio Technologies, Vista, CA) and subsequently contoured for Gleason score by a pathology assistant supervised by a genitourinary pathologist.

Registration

Coregistration of image data was necessary due to the deformation of the tissue, caused by differing geometries (rigid vs. inflatable) of the ER probes and the uncompressed nature of the ex vivo tissue. Contoured histology, sodium MRI data, ADC maps, and T_2-weighted contrast were compared after image coregistration through a previously reported registration pipeline.[26] This pipeline is schematically illustrated in Fig. 1, which presents representative coregistered imaging data. ADC is not included in the pipeline figure as it is inherently registered to the high-resolution T_2-weighted images. All manual registration was performed using 3D Slicer (v. 4.3.1) with a nonrigid, interactive thin-plate spline (TPS) extension. Registration involved positioning of ∼40 fiducial points on physiologically relevant regions of interest (ROIs), such as benign prostatic hyperplasia and cystic spaces, in the two image volumes being coregistered.[26] After fiducial points were finalized, an input and reference volume were chosen and the input volume was deformed to fit the reference volume according to the fiducial points chosen. The measured error for 3D histopathology reconstruction is 0.7 mm, with an overall in vivo MRI-histopathology coregistration error of ∼1.5 mm.[26]

Statistical Analysis

The histology contour masks were outlined on each histology slice were identified as either PIN, Gleason grade 3, Gleason score 3 + 4, Gleason score 4 + 3, or Gleason grade 4. These masks were then overlaid onto co-registered TSC and ADC maps as well as T_2 images to determine how the data obtained from each image set compares to identified regions of Gleason score. Distinct identified regions are classified in two ways: regions of Gleason pattern completely encapsulated by either healthy tissue or another Gleason score. Areas of patchy Gleason patterning were segmented into 4-mm^2 areas that contained only one Gleason score. TSC, ADC, and T_2-measurements were collected from four Gleason grades, prostatic intraepithelial neoplasia (PIN), and healthy peripheral zone (PZ) tissue. Healthy PZ tissue is designated as the remaining area of the PZ on the histology slides that has not been identified as cancerous by Gleason grading. The areas (mm^2) of Gleason contour coverage on whole-mount histology sections are displayed in Table 2. ADC data are presented as absolute ADC values, while TSC and T_2 data are presented as percent changes in TSC (ΔTSC) and T_2-weighted imaging contrast (ΔT_2). These values were calculated using Eqs. 1 and 2, respectively.

$$\Delta\mathrm{TSC} = 100\% \times \frac{(\mathrm{TSC}_{Lesion} - \mathrm{TSC}_{Healthy})}{\mathrm{TSC}_{Healthy}} \quad (1)$$

$$\Delta\mathrm{T}_2 = 100\% \times \frac{(\mathrm{T}_{2\,Lesion} - \mathrm{T}_{2\,Healthy})}{\mathrm{T}_{2\,Healthy}} \quad (2)$$

Using percent change of TSC and T_2 signal rather than absolute signal allows for more direct observation of changes in imaging

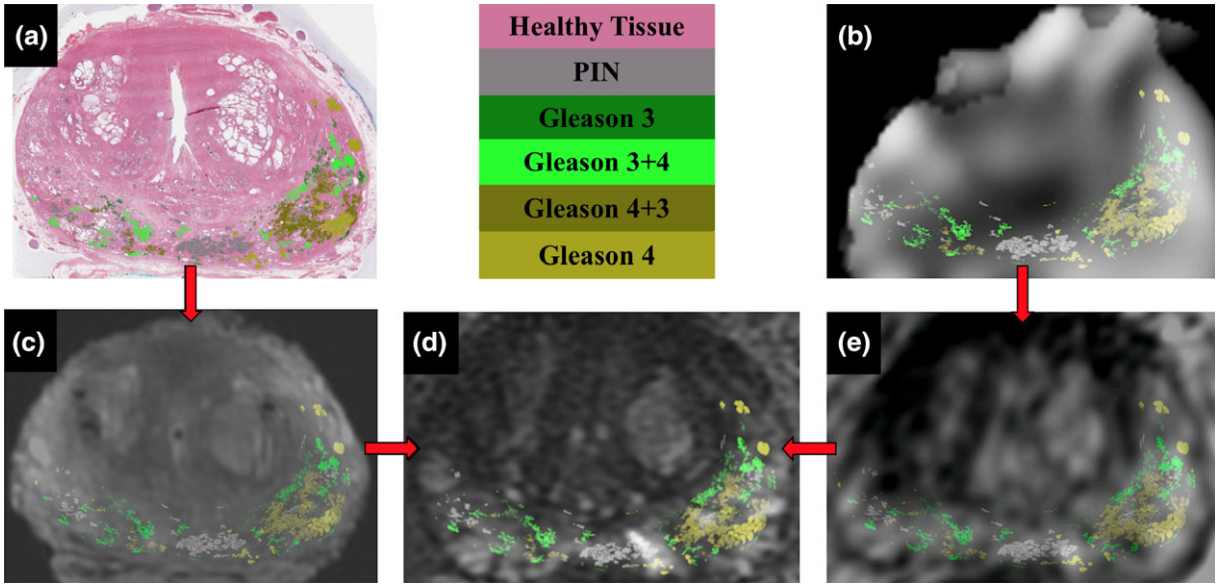

FIGURE 1: Registration pipeline for all imaging data with Gleason contours overlaid. Whole-mount histopathology (a) and the sodium-MR image (b) are registered to the T_2-weighted ex vivo (c) and the lower-resolution T_2-weighted in vivo images (e), respectively. The ex and in vivo images are individually registered to the high-resolution T_2-weighted in vivo image (d). Gleason contour legends are shown in the upper middle panel.

data related to the difference in lesion stage. Average in vivo sodium levels can be dependent on metabolic activity and perfusion, resulting in interpatient differences in baseline tissue sodium concentrations. Measurements of percent change assess how TSC and T_2-contrast vary from healthy tissue levels with increasing Gleason score in individual patient lesions.

All data were imported into GraphPad Prism v. 7.00 (GraphPad Software, La Jolla, CA) to test for significant differences in ΔTSC, ADC, and ΔT_2 values in relation to Gleason score for both individual patients and averaged data. Differences were tested using either a one-way analysis of variance (ANOVA) and a follow-up Tukey test or an unpaired *t*-test, depending on the number of Gleason grades present on that case's histology. For these statistical tests, the *n*-value used was equal to the number of identified voxels. SPSS statistical software v. 20.0.0 (IBM, Armonk, NY) was then used to perform a Spearman's nonparametric ranked correlation; testing the strength of the association between ΔTSC, ADC, and ΔT_2 values and Gleason score. For this test, the *n*-value represents the number of patients that had each Gleason score. A Pearson's parametric nonranked correlation was preformed between ΔTSC, ADC, and ΔT_2 data to assess the associations between these values. Error bars on individual patient graphs are standard error of the mean. Error bars on patient cohort graphs represent one standard deviation. Error bars on patient cohort graphs represent one standard deviation. Significance was measured at the 0.05 level.

Results

Clinically relevant patient data are given in Table 1. In the prostatectomy specimens acquired from the 10 cases, 564 distinct identified regions of Gleason-graded cancer were found in the PZ based on manual segmentations. The distribution of these identified regions on a per-patient basis is shown in Fig. 2. The measured areas of individual lesions ranged from 2.5–122 mm^2 on histological sections. Lesion measurement data are displayed in Table 2. We report that eight patients had clinically significant lesions (≥Gleason 7). One patient (patient 6) possessed a high prebiopsy PSA blood serum level but was excluded from statistical analysis because only one Gleason grade of cancer was found by pathology. Individual patient data for ΔTSC, ADC, and ΔT_2 are displayed in Table 2 and graphed as a function of Gleason grade in Supplementary Figs. 1–3, respectively. Calculation of standard deviations for ΔTSC, ADC, and ΔT_2 data involves a division by the differences between $TSC_{Healthy}$ and TSC_{Lesion}. Therefore, when these differences are small, the standard deviations increase. This accounts for the larger standard deviations in some cases.

Averaging all patient data showed a statistically significant increasing trend in ΔTSC with respect to Gleason score. Furthermore, statistically significant increases in ΔTSC within graded lesions were observable in the data from six of the nine patients ($p < 0.05$). Data from a representative patient is shown in Fig. 3, where significant differences were measured between all grades except Gleason 3 and 3 + 4 ($p < 0.01$). ΔTSC values from all ten patients are plotted in Figure 4a. These data were correlated with Gleason score using a Spearman's correlation. An r_s value of 0.791 was found showing a significant positive correlation ($p < 0.01$) (Figure 7). Weighted averages of ΔTSC were calculated for each Gleason score (Figure 4b). Averages were calculated from patient cohort data using weighting based on the number of voxels available for extraction of imaging data. Averaged data showed a monotonic increase in ΔTSC with Gleason score. Statistical analysis showed that all differences in average ΔTSC values between Gleason grades were

TABLE 1. Clinical Data for the 10 Patients Analyzed in the Study

Category	Patient 1	Patient 2	Patient 3	Patient 4	Patient 5	Patient 6	Patient 7	Patient 8	Patient 9	Patient 10
Age	65	64	53	66	64	66	68	59	57	66
Pretreatment procedures										
Prebiopsy PSA (ng/mL)	14.96	5.05	4.22	6.13	4.33	25.49	4.66	3.67	1.05	4.16
Primary pattern	3	3	3	3	4	4	3	3	3	3
Secondary pattern	4	4	4	4	3	4	4	4	4	3
Overall Gleason score	7	7	7	7	7	8	7	7	7	6
Prostate volume (cc)	45	30	25	65	39	57	23	22.6	48.32	37
Clinical T-Stage	cT2c	cT2c	cT1c	cT2b	cT1c	cT2a	cT2b	cT1c	cT1c	cT2a
Screening bloodwork										
Creatinine (µmol/L)	76	64	92	90	84	69	105	69	77	75
eGFR (mL/min/1.73m^2)	95	116	79	78	85	106	65	108	96	96
Urea (mmol/L)	5.1	3.9	6.9	5.2	9.2	5	9.1	6.1	6.5	6.1
Residual bladder volume (mL)	78	224	165	49	20	18	0	32	92	0
Post radical prostatectomy										
Primary pattern	3	3	3	3	4	3	3	3	3	3
Secondary pattern	4	4	4	4	3	4	4	4	4	4
Tertiary pattern	5	None	None	5	None	None	None	None	None	None
Overall Gleason score	7	7	7	7	7	7	7	7	7	7
Pathological T-Stage	pT3b	pT3a	pT2c	pT3b	pT3a	pT3a	pT2c	pT2c	pT2c	pT2c
Pathological N-Stage	pN0	pN0	pN0	pN0	pN0	pN0	pN0	pN0	pN0	pNX
Pathological P-Stage	pMx	pMx	pMx	pMx	pMx	pMx	pMx	pMx	pMx	pMx

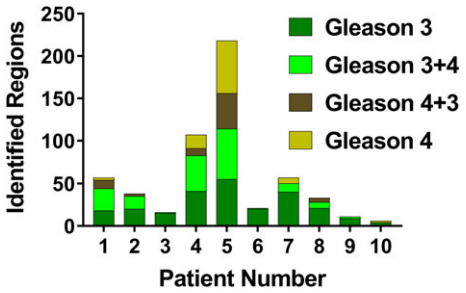

FIGURE 2: The number and distribution of identified regions of prostate cancer is shown in each of the 10 patients. The identified regions were manually segmented on accurately coregistered whole-mount histopathology using a method described in the Statistical Analysis section.

significant ($p < 0.001$). It was observed that the differences in ΔTSC between adjacent Gleason grades becomes larger as identified cancer increases in stage.

ADC values were also compared to Gleason score. Significance was recorded between Gleason grades in seven of nine patients. However, a nonmonotonic trend between ADC and Gleason score was observed in individual patients (Supplemental Fig. 2) and cohort data (Fig. 5a). A Spearman's correlation test identified a nonsignificant correlation of ADC with Gleason score ($r_s = -0.306$, $p = 0.079$) (Fig. 7). Weighted averages of ADC data were calculated from each Gleason score (Fig. 5b). Nonmonotonic, significant differences in ADC values were observed between all the Gleason grades ($p < 0.05$).

ΔT_2 data were compared to Gleason score, showing significant changes in seven of the nine individual patients ($p < 0.05$). A Spearman's correlation was performed on data from the patient cohort (Fig. 6a), showing a nonsignificant correlation between ΔT_2 and Gleason grade ($r_s = -0.069$, $p = 0.699$) (Fig. 7). Weighted averages of ΔT_2 data exhibited nonmonotonic, significant differences between Gleason scores (Fig. 6b).

We tested for associations between our imaging data using a Pearson correlation. We observed a statistically significant correlation between ADC and ΔT_2 data ($r = 0.472$, $p = 0.005$). However, ΔTSC was not correlated with either ADC or ΔT_2 ($r = 0.058$, $p = 0.371$, and $r = -0.158$, $p = 0.745$, respectively).

Discussion

We report in vivo measurements of tissue sodium concentration in human PCa. In addition, this work also represents the first correlation of changes in tissue sodium concentration acquired with sodium MRI to histologically confirmed Gleason grade using a validated image registration pipeline. Our data show a statistically significant monotonic increase in ΔTSC with increasing Gleason score for individual patients and cohort-averaged patient data. This provides preliminary evidence for the use of sodium MRI as a noninvasive approach to characterize prostate lesions.

Previously, we demonstrated that TSC can be measured in the human prostate with sufficient signal-to-noise ratio (SNR).[24] The reference standard for PCa diagnosis involves a TRUS-guided 12-core biopsy, sampling a small fraction of the volume of the entire prostate gland. Uncertainty that arises after negative biopsies due to undersampling of potentially aggressive lesions is a major concern for physicians when assigning men to active surveillance. Low-risk, Gleason 6 cancer is the most common diagnosis after biopsy; this grade rarely metastasizes and has a very small associated mortality. This study demonstrates that sodium MRI of the prostate could provide additional reliable information to noninvasively characterize prostate lesions for risk stratification decisions. Patients with lower-risk lesions could be confidently monitored with active surveillance, which might include sodium MRI, whereas patients in the high-risk category (≥Gleason 7) would receive treatment as prescribed by the National Comprehensive Cancer Network's guidelines.[27] Gleason 7 patients with low-volume Gleason 3 + 4 PCa are excluded from an immediate treatment recommendation[28] and would benefit from whole-gland lesion characterization by TSC measurement. More reliable noninvasive identification of biologically significant foci in the gland may enable clinical decisions including targeted biopsy, focal therapy, or focal dose-escalation strategies.[29–32]

This study involved the development of advanced MRI hardware and a comprehensive data analysis including 3D registration of whole-mount digital histopathology to multiple mpMRI contrasts with a high degree of accuracy (~2 mm). Accurate image registration is imperative to assure that the TSC data measured in a specific ROI are being accurately associated with the Gleason contours on digital histology. This pipeline is explained in the methods section. Finally, the development of sensitive integrated RF hardware for sodium imaging was an important development for PCa research.[24] The current study shows that ΔTSC increases with Gleason grade, and this trend was present in both individual datasets and cohort-averaged data. This increasing trend showed a strong significant correlation with Gleason score ($p < 0.01$), while data from ADC and ΔT_2 did not show strong correlations (Fig. 7). While we are unable to associate the ΔTSC correlation with specific cellular changes, it is likely due to cellular reorganization (volume changes) and increased intracellular sodium concentration.[18] With increasing Gleason score, cellular density increases, which leads to a decreased extracellular volume. Cancer cells have been shown to exhibit an increased metabolism, which supplies the cell with enough energy to support accelerated proliferation and enhanced motility.[33] The caveats of this increased metabolism include an upregulation of the sodium-proton (Na^+/H^+) antiport[19,20] and inhibition of a sodium-potassium (Na^+/K^+-ATPase) pump.[21,34] As the tumor cell favors aerobic glycolysis (glycotic energy production over oxidative phosphorylation, even in

TABLE 2. Percent Changes in TSC (ΔTSC), ADC Values, and Percent Changes in T_2-signal (ΔT_2) for All 10 Patients

Case	TSC percent change, ADC values, T_2 percent change for all patients																			
	PIN				Gleason 3				Gleason 3 + 4				Gleason 4 + 3				Gleason 4			
	Histology Area (mm^2)	ΔTSC (%)	ADC (×10^{-6} mm^2/s)	ΔT_2 (%)	Histology Area (mm^2)	ΔTSC (%)	ADC (×10^{-6} mm^2/s)	ΔT_2 (%)	Histology Area (mm^2)	ΔTSC (%)	ADC (×10^{-6} mm^2/s)	ΔT_2 (%)	Histology Area (mm^2)	ΔTSC (%)	ADC (×10^{-6} mm^2/s)	ΔT_2 (%)	Histology Area (mm^2)	ΔTSC (%)	ADC (×10^{-6} mm^2/s)	ΔT_2 (%)
Patient 1	88	12.5 ± 16	1271 ± 182	−22 ± 30	199	−3.4 ± 17	1175 ± 84	18 ± 29	608	5.9 ± 14	1178 ± 86	−12 ± 29	1173	14.1 ± 20	1041 ± 45	−17 ± 31	3	37.6 ± 15	1372 ± 105	−21 ± 29
Patient 2	881	−12.5 ± 38	1435 ± 137	−7 ± 46	133	−11.3 ± 28	1944 ± 49	−12 ± 45	573	7.6 ± 37	1554 ± 53	−11 ± 46	72	32.8 ± 32	1256 ± 52	16 ± 46				
Patient 3	340	−6.3 ± 45	1159 ± 88	−17 ± 11	39	16.9 ± 38	1801 ± 100	−24 ± 12	21	38.8 ± 39	1746 ± 19	39 ± 12								
Patient 4	95	4.4 ± 22	1231 ± 137	−33 ± 6	21	13.3 ± 20	1281 ± 61	−16 ± 5	173	3.9 ± 22	1027 ± 29	−37 ± 6	9	23.7 ± 19	675 ± 25	−38 ± 6	8	58 ± 28	1137 ± 17	−33 ± 6
Patient 5	321	−1.4 ± 56	1335 ± 110	20 ± 88	101	13.7 ± 45	1408 ± 102	17 ± 84	175	17.2 ± 48	1254 ± 145	15 ± 85	386	33.5 ± 58	1424 ± 38	9 ± 87	250	44.5 ± 58	1504 ± 85	12 ± 87
Patient 6					8	16.7 ± 22	1750 ± 100	−16 ± 7												
Patient 7	10	−33 ± 98	1669 ± 175	3 ± 12	13	16.3 ± 93	1742 ± 50	4 ± 5									3	30.2 ± 92	1229 ± 67	−8 ± 6
Patient 8	27	−2.8 ± 89	1421 ± 107	−16 ± 10	15	5 ± 88	1352 ± 78	−25 ± 10												
Patient 9	620	10 ± 458	1358 ± 96	−4 ± 4	39	13.3 ± 252	1268 ± 128	−3 ± 3	15	19 ± 249	1200 ± 128	−21 ± 3								
Patient 10	129	−7.4 ± 42	1159 ± 88	−35 ± 7	3	8.2 ± 28	1124 ± 281	−4 ± 8									3	18 ± 28	787 ± 49	−74 ± 8
Average		−2.9 ± 34	1327 ± 24	−9 ± 34		1.9 ± 18	1469 ± 40	−2 ± 16		8.1 ± 31	1350 ± 17	−8 ± 31		19.5 ± 43	1159 ± 11	−8 ± 43		44.4 ± 22	1352 ± 27	−23 ± 22

Data are displayed as ΔTSC, ADC, or ΔT_2 ± standard deviation. The size of the Gleason contour from which the imaging data was extracted is shown on the left side of each column (mm^2). Weighted averages for all patient data are shown at the bottom of the table with standard deviation.

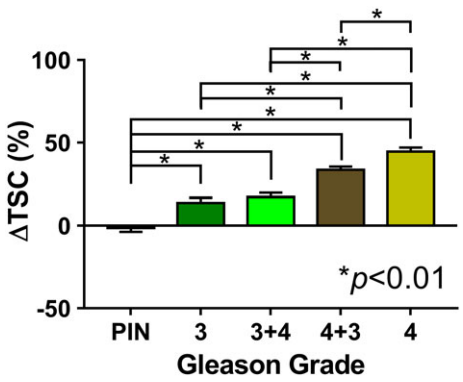

FIGURE 3: ΔTSC in relation to Gleason grade for a representative case (Patient 5) from our patient cohort of 10. Error bars represent standard error of the mean.

the presence of oxygen),[35] this leads to an accumulation of protons within the cell, reducing pH. Na^+/H^+ antiport is the major mechanism used to reduce the concentration of intracellular protons.[17] As protons are pumped out, sodium moves into the cell, increasing its intracellular concentration. An acidic extracellular environment is also favored by the cancer cells, as it aids in cell motility[36] and invasiveness.[37]

In this study we preformed DWI in conjunction with mpMRI and sodium MRI. Our DWI data shows that ADC values were not as strongly correlated with Gleason score as were sodium data. Data from individual patient, patient cohort data, and cohort average data showed little association between ADC measurements and Gleason score. The ADC measurements recorded in this study agreed with values previously reported in PCa by Hambrock et al.[11] A previous study has shown that ADC can be used as an imaging biomarker of cell density in glioma, ovarian, and lung cancer; however, only moderate correlations were seen in PCa between ADC and cell density.[15] Other research has demonstrated limitations in characterizing dispersed prostatic lesions from normal tissue in the PZ using T_2-signal change.[38] This study examined changes in T_2-weighted contrast in relation to Gleason grade. Changes in T_2-weighted contrast in the prostate can be due to many factors. Kirkham et al[16] showed that benign abnormalities like chronic prostatitis, hyperplasia, scars, atrophy, and postbiopsy hemorrhage all lead to lower signal intensity in T_2-weighted images. We observed a weak and nonsignificant correlation coefficient between ΔT_2 data and Gleason score; however,

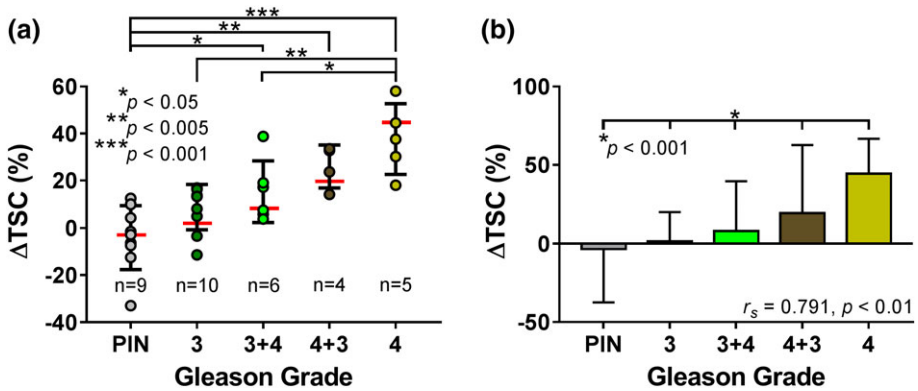

FIGURE 4: ΔTSC in relation to Gleason score. (a) Patient cohort data. Horizontal red line indicates weighted average of all data points. Error bars represent standard deviation. Value of *n* represents the number of patients that possessed a particular Gleason score out of the cohort of 10. (b) Weighted average of ΔTSC data; error bars represent one standard deviation. The r_s values shown represents the Spearman's correlation coefficient.

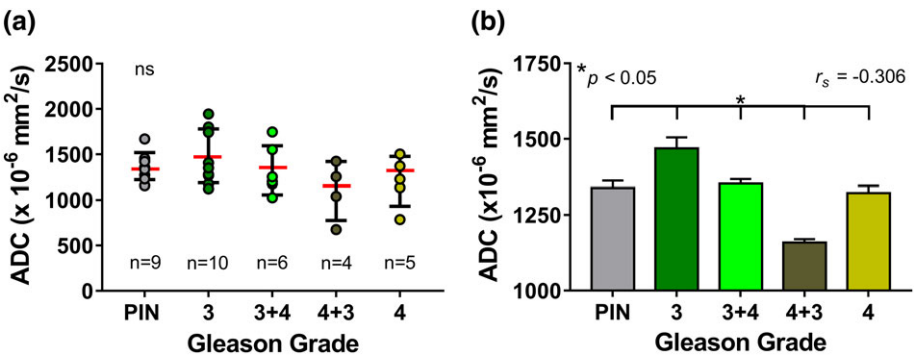

FIGURE 5: ADC measurements in relation to Gleason score. (a) Patient cohort data. Horizontal red line indicates weighted average of all data points. Error bars represent standard deviation. Value of *n* represents the number of patients that possessed a particular Gleason score out the cohort of 10. (b) Weighted average of ADC data; error bars represent one standard deviation. The r_s value shown represents the Spearman's correlation coefficient. ns denotes no significance.

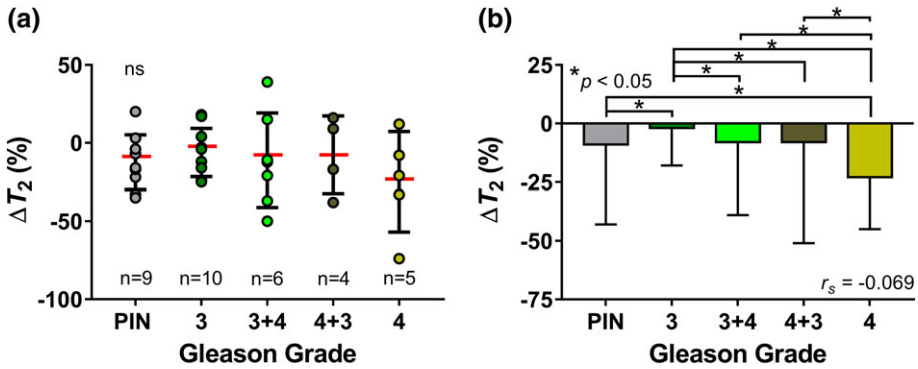

FIGURE 6: ΔT_2 in relation to Gleason score. (a) Patient cohort data. Horizontal red line indicates weighted average of all data points. Error bars represent standard deviation. Value of *n* represents the number of patients that possessed a particular Gleason score out the cohort of 10. (b) Weighted average of ΔT_2 data, error bars represent one standard deviation. The r_s value shown represents the Spearman's correlation coefficient. ns denotes no significance.

all averaged ΔT_2 data in lesions were negative, indicating that signal did decrease in lesions compared to healthy tissue. This result has been reported in the literature.[39] The decrease in T_2 signal was not correlated with Gleason grade. Patient cohort data displayed a statistically significant correlation between ADC and ΔT_2. Comparisons between ADC and T_2-contrast have been reported in the literature with similar results.[39] Additionally, we showed that ADC and ΔT_2 were both not significantly associated with TSC. The correlation between ADC and ΔT_2 is likely a correlation between cellular density measurements. However, cell density information alone doesn't necessarily provide reliable characterization of a lesion.[38] The addition of ΔTSC to supplement mpMRI has the potential for noninvasive lesion characterization. Further, ΔTSC could have translational potential to help direct image-guided biopsy. Sodium MRI affords clinicians accurate, noninvasive lesion classification; this may help with biopsy needle trajectory planning, decreasing undersampling of clinically significant foci and repeated negative biopsies.

There are several limitations to this study that bear discussion. This preliminary study involved 10 men with biopsy-proven PCa; however, an average of 60 distinct lesions were identified per patient on histological prostate sections after prostatectomy. In total, 243 Gleason 3, 163 Gleason 3 + 4, 68 Gleason 4 + 3, and 90 Gleason 4 prostate lesions were identified from this cohort of patients and included in the statistical analysis. As a result, regardless of the limited number of men in this study, a statistically significant correlation between ΔTSC and Gleason score was observed for the entire cohort and in individual patient data. In the current study, the spatial resolution of sodium MRI was ~5 mm^3 vs. ~0.5 mm^3 for proton imaging. A broad-banded fast gradient-recalled-echo pulse sequence with a Cartesian *k*-space trajectory was employed in this study. 3D-spiral or radial pulse sequences, which are optimized for fast T_2 relaxation and efficient coverage of *k*-space for sodium MRI, have demonstrated the potential for improved SNR.[40] Further development in this area could potentially increase spatial resolution and/or reduce acquisition times for sodium MRI in the prostate. An inherent limitation of a surface ER coil is the receive profile, in which the signal requires sensitivity correction due to the inhomogeneous receive profile. This is an issue for all prostate MRI (including ^{1}H MR), where high-resolution imaging often requires the use of an ER coil. Our ΔTSC data were corrected for the sensitivity profile of the rigid sodium ER coil before analysis to help ameliorate this problem. The same correction was not performed on ΔT_2 data, which were acquired with a separate inflatable (nonrigid) ^{1}H ER coil. As a result, these data may be subject to small errors. Prostate lesions were identified in both the peripheral and central zones; however only those within the peripheral zone were measured for this study. The close proximity of the PZ to the ER coil reduces the possible error in ΔT_2 data without sensitivity correction. Future work can look at previously acquired DCE imaging data, comparing metrics from the gadolinium-enhanced contrast to the accurately coregistered histological Gleason contours.

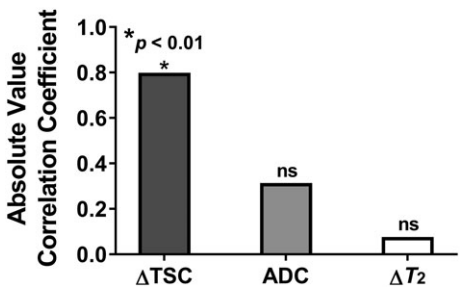

FIGURE 7: Absolute values of Spearman's nonparametric ranked correlation coefficients for ΔTSC, ADC, and ΔT_2 data. Correlations were performed between imaging data and Gleason grade. No significance denoted by ns.

In conclusion, this research demonstrated statistically significant increases in in vivo ΔTSC with increasing Gleason grade in individual patients. Accurate assessment of lesions on an individual basis is important if sodium MRI is to be used to characterize tumor grade clinically. Further, a strong correlation

was found between ΔTSC and Gleason score in patient cohort data along with monotonic, statistically significant increases in ΔTSC when cohort data were averaged together. The combination of sodium MRI with mpMRI to form a noninvasive imaging assay promises improved detection, characterization, and surveillance of prostate lesions, which will ultimately increase the confidence of men with early-stage disease to choose active surveillance instead of radical treatment.

Acknowledgments

Grant sponsor: Ontario Institute for Cancer Research, Smarter Prostate Imaging Program (to R.B. and T.J.S.); Grant sponsor: The Natural Sciences and Engineering Research Council of Canada (Discovery Grant to T.J.S.).

We acknowledge the valuable assistance of Clinical Research Associates, Ashley Foster and Stephanie Horst, with patient recruitment and research assistance, Cathie Crukley, for preparation of the prostates for ex vivo imaging and pathology. We also thank Professor Wenqing He for input with the statistical analysis of our data. We thank the members of the Translational Imaging Research Facility at the Robarts Research Institute, including MR Technologists, Dave Reese and Trevor Szekeres, for assistance imaging the patients used in this study. Finally, we would also like to acknowledge the contributions of Dr. Cesare Romagnoli, who was instrumental in fostering this research in its infancy and who has left us much too soon. He is missed by all his collaborators. We dedicate this article to his memory.

References

1. Statistics CC. Statistics CCSAC on Cancer Statistics. 2017.
2. Draisma G, Etzioni R, Tsodikov A, et al. Lead time and overdiagnosis in prostate-specific antigen screening: importance of methods and context. J Natl Cancer Inst 2009;101:374–383.
3. Heijnsdijk, E.A., A. der Kinderen, E.M. Wever, et al. Overdetection, overtreatment and costs in prostate-specific antigen screening for prostate cancer. Br J Cancer, 2009;101:1833–1838.
4. Dragomir, A., F.L. Cury, and A.G. Aprikian, Active surveillance for low-risk prostate cancer compared with immediate treatment: a Canadian cost comparison. CMAJ Open, 2014;2:E60–68.
5. Taira, A.V., G.S. Merrick, R.W. Galbreath, et al. Performance of transperineal template-guided mapping biopsy in detecting prostate cancer in the initial and repeat biopsy setting. Prostate Cancer Prostatic Dis, 2010; 13:71–77.
6. Gordetsky, J. and J. Epstein, Grading of prostatic adenocarcinoma: current state and prognostic implications. Diagn Pathol, 2016;11:25.
7. Epstein, J.I., M.B. Amin, V.E. Reuter, et al. Contemporary Gleason Grading of Prostatic Carcinoma: An Update With Discussion on Practical Issues to Implement the 2014 International Society of Urological Pathology (ISUP) Consensus Conference on Gleason Grading of Prostatic Carcinoma. Am J Surg Pathol, 2017;41:e1–e7.
8. Scattoni, V., A. Zlotta, R. Montironi, et al. Extended and saturation prostatic biopsy in the diagnosis and characterisation of prostate cancer: a critical analysis of the literature. Eur Urol, 2007;52:1309–1322.
9. Sedelaar, J.P., P.L. Vijverberg, T.M. De Reijke, et al. Transrectal ultrasound in the diagnosis of prostate cancer: state of the art and perspectives. Eur Urol, 2001;40:275–284.
10. Djavan, B., V. Ravery, A. Zlotta, et al. Prospective evaluation of prostate cancer detected on biopsies 1, 2, 3 and 4: when should we stop? J Urol, 2001;166:1679–1683.
11. Hambrock, T., D.M. Somford, H.J. Huisman, et al. Relationship between Apparent Diffusion Coefficients at 3.0-T MR Imaging and Gleason Grade in Peripheral Zone Prostate Cancer. Radiology, 2011;259:453–461.
12. Hoeks, C.M., J.O. Barentsz, T. Hambrock, et al. Prostate cancer: multiparametric MR imaging for detection, localization, and staging. Radiology, 2011;261:46–66.
13. Weidner, A.M., H.J. Michaely, A. Lemke, et al. Value of multiparametric prostate MRI of the peripheral zone. Z Med Phys, 2011;21:198–205.
14. Fornasa, F., Diffusion-weighted Magnetic Resonance Imaging: What Makes Water Run Fast or Slow? J Clin Imaging Sci, 2011;1:27.
15. Surov, A., H.J. Meyer, and A. Wienke, Correlation between apparent diffusion coefficient (ADC) and cellularity is different in several tumors: a meta-analysis. Oncotarget, 2017;8:59492–59499.
16. Kirkham, A.P., M. Emberton, and C. Allen, How good is MRI at detecting and characterising cancer within the prostate? Eur Urol, 2006;50: 1163–1174; discussion 1175.
17. Demaurex, N. and S. Grinstein, Na+/H + antiport: modulation by ATP and role in cell volume regulation. J Exp Biol, 1994;196:389–404.
18. Ouwerkerk, R., K.B. Bleich, J.S. Gillen, et al. Tissue sodium concentration in human brain tumors as measured with 23Na MR imaging. Radiology, 2003;227:529–537.
19. Reshkin, S.J., A. Bellizzi, S. Caldeira, et al. Na +/H + exchanger-dependent intracellular alkalinization is an early event in malignant transformation and plays an essential role in the development of subsequent transformation-associated phenotypes. FASEB J, 2000;14:2185–2197.
20. Rotin, D., D. Steele-Norwood, S. Grinstein, et al. Requirement of the Na +/H + exchanger for tumor growth. Cancer Res, 1989;49:205–211.
21. Kometiani, P., L. Liu, and A. Askari, Digitalis-induced signaling by Na+/K+-ATPase in human breast cancer cells. Mol Pharmacol, 2005;67:929–936.
22. Ouwerkerk, R., M.A. Jacobs, K.J. Macura, et al. Elevated tissue sodium concentration in malignant breast lesions detected with non-invasive 23Na MRI. Breast Cancer Res Treat, 2007;106:151–160.
23. Bartha, R., J.F. Megyesi, and C.J. Watling, Low-grade glioma: correlation of short echo time 1H-MR spectroscopy with 23Na MR imaging. AJNR Am J Neuroradiol, 2008;29:464–470.
24. Farag, A., J.C. Peterson, T. Szekeres, et al. Unshielded asymmetric transmit-only and endorectal receive-only radiofrequency coil for (23) Na MRI of the prostate at 3 tesla. J Magn Reson Imaging, 2015;42:436–445.
25. Axel, L., J. Costantini, and J. Listerud, Intensity correction in surface-coil MR imaging. AJR Am J Roentgenol, 1987;148:418–420.
26. Ward, A.D., C. Crukley, C.A. McKenzie, et al. Prostate: registration of digital histopathologic images to in vivo MR images acquired by using endorectal receive coil. Radiology, 2012;263:856–864.
27. National Comprehensive Cancer, N., Prostate cancer. NCCN clinical practice guidelines in oncology. J Natl Compr Canc Netw, 2004;2: 224–248.
28. Morash, C., R. Tey, C. Agbassi, et al. Active surveillance for the management of localized prostate cancer: Guideline recommendations. Can Urol Assoc J, 2015;9:171–178.
29. Kanthabalan, A., M. Emberton, and H.U. Ahmed, Biopsy strategies for selecting patients for focal therapy for prostate cancer. Curr Opin Urol, 2014;24:209–217.
30. van den Bos, W., B.G. Muller, H. Ahmed, et al. Focal therapy in prostate cancer: international multidisciplinary consensus on trial design. Eur Urol, 2014;65:1078–1083.

31. Kasivisvanathan, V., M. Emberton, and H.U. Ahmed, Focal therapy for prostate cancer: rationale and treatment opportunities. Clin Oncol (R Coll Radiol), 2013;25:461–473.

32. Bauman, G., M. Haider, U.A. Van der Heide, et al. Boosting imaging defined dominant prostatic tumors: a systematic review. Radiother Oncol, 2013;107:274–281.

33. Langer, D.L., T.H. van der Kwast, A.J. Evans, et al. Prostate tissue composition and MR measurements: investigating the relationships between ADC, T2, K(trans), v(e), and corresponding histologic features. Radiology, 2010;255:485–494.

34. Cameron, I.L., N.K. Smith, T.B. Pool, et al. Intracellular concentration of sodium and other elements as related to mitogenesis and oncogenesis in vivo. Cancer Res, 1980;40:1493–1500.

35. Vander Heiden, M.G., L.C. Cantley, and C.B. Thompson, Understanding the Warburg effect: the metabolic requirements of cell proliferation. Science, 2009;324:1029–1033.

36. Goetze, K., S. Walenta, M. Ksiazkiewicz, et al. Lactate enhances motility of tumor cells and inhibits monocyte migration and cytokine release. Int J Oncol, 2011;39:453–463.

37. Kato, Y., S. Ozawa, C. Miyamoto, et al. Acidic extracellular microenvironment and cancer. Cancer Cell Int, 2013;13:89.

38. Langer, D.L., T.H. van der Kwast, A.J. Evans, et al. Intermixed normal tissue within prostate cancer: effect on MR imaging measurements of apparent diffusion coefficient and T2—sparse versus dense cancers. Radiology, 2008;249:900–908.

39. Gibbs, P., G.P. Liney, M.D. Pickles, et al. Correlation of ADC and T2 measurements with cell density in prostate cancer at 3.0 Tesla. Invest Radiol, 2009;44:572–576.

40. Nielles-Vallespin, S., M.A. Weber, M. Bock, et al. 3D radial projection technique with ultrashort echo times for sodium MRI: clinical applications in human brain and skeletal muscle. Magn Reson Med, 2007;57:74–81.